Optics Communications 333 (2014) 232–236

Contents lists available at ScienceDirect

Optics Communications

journal homepage: www.elsevier.com/locate/optcom

Characterization of photonic bands in metal photonic crystal slabs

Lin Chen*, Khanh Viet Truong, Zhaoxiang Cheng, Zhou Li, Yiming Zhu*

Engineering Research Center of Optical Instrument and System, Ministry of Education, Shanghai Key Lab of Modern Optical System, University of Shanghai for Science and Technology, No. 516 JunGong Road, Shanghai 200093, China

ARTICLE INFO

Article history:
Received 5 June 2014
Received in revised form
7 July 2014
Accepted 14 July 2014
Available online 25 July 2014

Keywords:
Metal photonic crystal
Terahertz
Photonic band
Dispersion

ABSTRACT

By rotating metal photonic crystal (PC) slab around ΓK and ΓM lattice directions, transmission spectra were measured to study photonic bands in such metal PC with a triangular lattice. We found that the photonic band diagram for the ΓM lattice direction is different from that for the ΓK direction. Approximate formulas of angular-dependent resonant frequencies are derived to quantitatively analysis the dispersion of metal PC. Furthermore, experimental results for the dominant resonances of (−1, 0) (ΓM) and (0,−1) (ΓK) confirm the accurate of formulas. All these results can be used to analyze and design devices based on metal PC.

1. Introduction

Photonic crystal (PC) slabs, which often refer to two dimensional PC with finite thickness, have been widely concerned due to their potential to control the propagation of electromagnetic waves [1]. In terahertz (THz) range, as the fabrication of PC is much more convenient than that at optical frequencies, increasing interest in the use of PC has been seen for many applications. Lots of research focused on the transmission properties for out-of-plane propagations through silicon PC due to the low loss property of silicon in THz range. From the angular variation of the transmission spectra, the photonic band structure for the guided resonances can be found, which can benefit to the development of photonic devices [2–5]. Compared with the silicon PC, the metal PC slabs (also called metal holes array, MHA) show the unique characteristics in the microwave and THz range due to their influence on the electric field of electromagnetic wave. Extraordinary transmission phenomenon has been sufficiently studied through such metal PC slabs which can be applied to filters and sensors [6–8]. One can find systematic introduction of metal PC (or MHA) in some review articles [9,10]. More recently, the dispersion curves of spoof surface plasmons (SPs) and photonic band structures in metal PC are discussed in microwave and THz range for the propose of extraordinary transmission [11–13]. However, they all focused on the metal PC slabs with a square lattice. Interestingly, such dispersion characteristics of SPs for long range and short range in a triangular array of holes have been studied in visible region and the photonic bands have been clearly found by the angle-resolved spectra [14]. In this paper, we use the method proposed in Ref. [3] to analysis the THz photonic band diagrams for the ΓM and ΓK directions in metal PC with a triangular lattice and verify the dominant dispersions by rotating the sample with ΓM and ΓK directions. Analytic formulas of resonant frequencies for two lattice directions are derived based on the momentum conservation theory. Compared with metal PC slabs with a square lattice, the band structure for the ΓM direction is different from that for the ΓK direction. The dominant resonant frequencies experimentally observed show good agreement with results from formulas. Our results should inspire further interest in the development of metal photonic devices.

2. Experimental results and discussion

The proposed metal PC consisted of a triangular array of circle air holes in an aluminum plate with the parameters of $t = 0.25$ mm, $d = 0.7$ mm, and $p = 1.13$ mm, as shown in Fig. 1(a). To study photonic band, we employ an out-of-plane illumination scheme (Fig. 1(b)), which is similar to the experimental setup of the silicon PC [3,4]. The ΓM and ΓK directions are also shown in Fig. 1(b). The metal PC has geometry with size of 50 mm in order to provide sufficient periodical extension and nearly infinite boundary condition [15].

The transmission measurement was carried out using a terahertz time domain spectroscopy (THz-TDS) system [15–17]. A collimated THz wave, which was radiated from the emitter of a photoconductive antenna pumped by a 100-fs 800 nm laser

* Corresponding authors. Tel./fax: +86 2133773176.
E-mail addresses: linchen@usst.edu.cn (L. Chen), ymzhu@usst.edu.cn (Y. Zhu).

http://dx.doi.org/10.1016/j.optcom.2014.07.045
0030-4018/

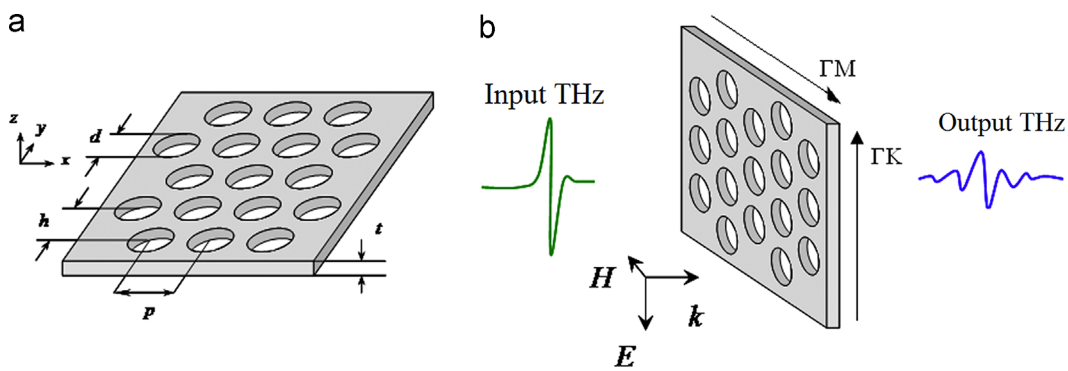

Fig. 1. (a) Overview of the metal PC slab. The crystal parameters of this sample are $d = 700$ μm, $p = 1.13$ mm and $t = 250$ μm. (b) Schematic of the experimental arrangement. At the incident angle θ corresponding to the normal of the slab, the in-plane component of the wave vector of the incident THz wave is along the ΓM or ΓK directions of triangular lattice.

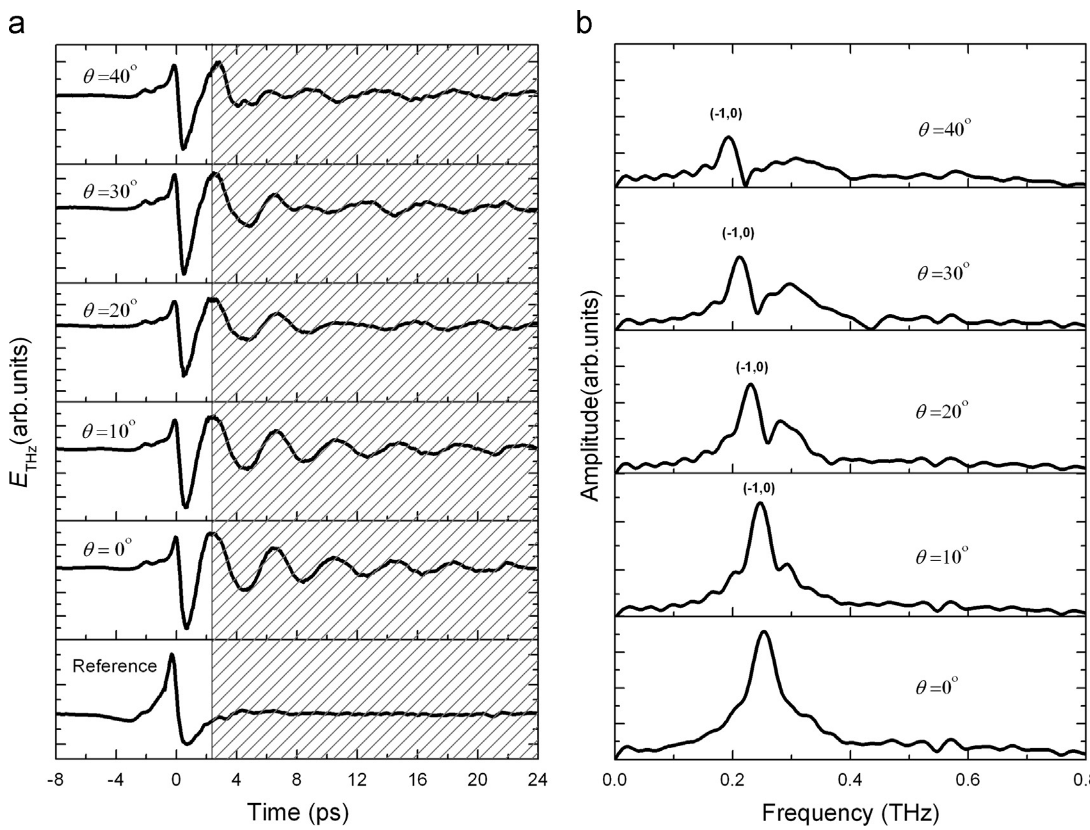

Fig. 2. (a) The incident THz wave form and THz wave forms transmitted through the metal PC along the ΓM direction. (b) Corresponding Fourier-transformed spectra in the time range after 2.5 ps.

pulse, was irradiated on the sample. By changing the time delay between the pumping and probe pulses, the wave form of the electric field of the transmitted THz wave could be measured. The sample with triangular arrays has two lattice directions: ΓM and ΓK (see Fig. 1(b)). p-polarized THz pulses were incident at the angle θ relative to the surface normal of the slab. The THz spot size is larger than the lattice constant of the metal PC, so many holes could be illuminated. A reference measurement was taken when there was no sample present, which we referred to as an air signal.

We measured the time domain waveforms of the metal PC at normal angle ($\theta = 0^\circ$ in Fig. 2(a)) and found that each wave form has an initial fast pulse and a long decaying tail. Since SP resonances are modes that are not confined inside the metal PC slab, they decay out of the slab with various lifetimes. To evaluate the frequency of such oscillation components, we made Fourier transformations of the waves form in the range after 2.5 ps, where the oscillation component appeared ($\theta = 0^\circ$ in Fig. 2(b)). The transmission peak at normal angle is observed at 0.26 THz. Then, we also experimentally studied the effects of the angle of incidence on the transmitted time-domain waveforms in ΓK (Fig. 2(a)) and ΓM (Fig. 3(a)) directions. When the incident angle θ becomes finite, after 2.5 ps the oscillation components are weak with the increase of the incident angle in ΓK and ΓM directions. This seems to be a consequence of lack of symmetry along the incident direction. Their transmission spectra are illuminated in Figs. 2(b)

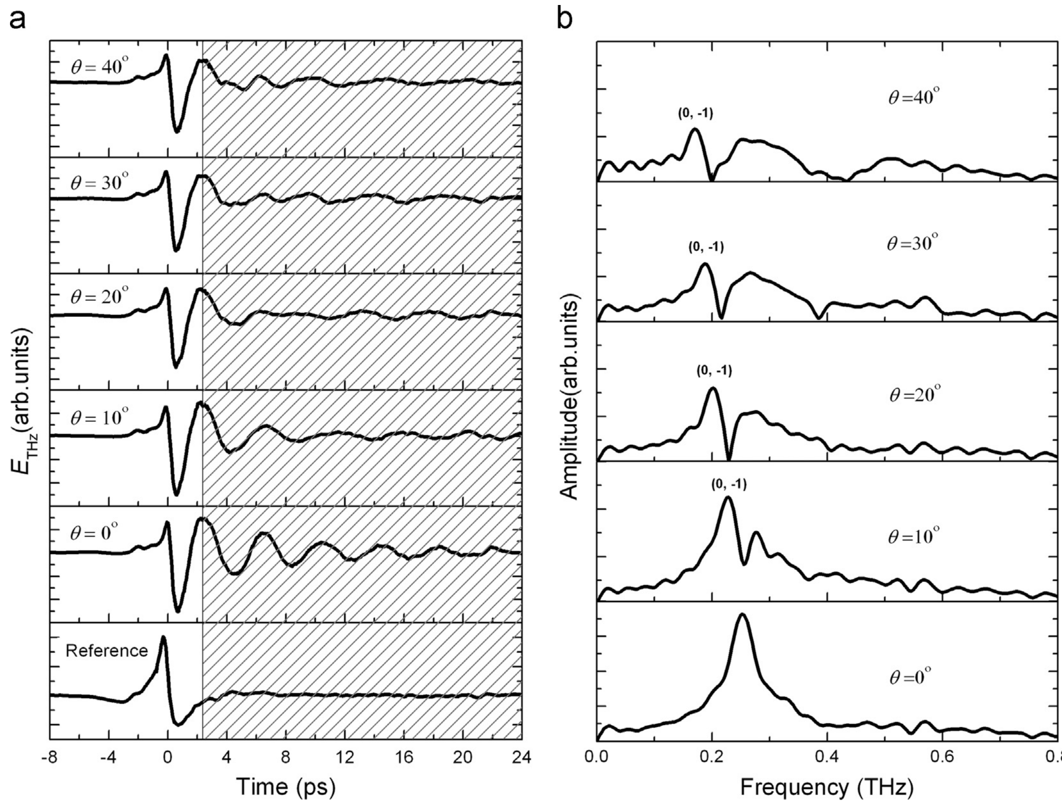

Fig. 3. (a) The incident THz wave form and THz wave forms transmitted through the metal PC along the ΓK direction. (b) The Fourier-transformed intensity of the THz wave form in the time range after 2.5 ps.

and 3(b) by taking the Fourier transformations after 2.5 ps. We found that the peak of the lowest resonant frequency moved toward low frequency direction and additional peaks emerged as the incident angle increases. In addition, the spectra with rotating around the ΓM direction are different from results with rotating around the ΓK direction at the same incident angle.

Next, we discuss the mechanism of the transmission spectra of the metal PC from results in Figs. 2 and 3. Considering energy and momentum conservation in the interaction between the PC momentums and the incident THz wave, if the THz wave is incident on a metal PC with a grating constant p at certain angle θ, the component of the wave vector $\overrightarrow{k}_{sur}$ on the surface can have a wave vector [9]

$$|\overrightarrow{k}_{sur}| = |\overrightarrow{k}_{x} + m\overrightarrow{G}_{x} + n\overrightarrow{G}_{y}|, \quad (1)$$

where m and n are integers; $\overrightarrow{k}_{x}$ is the component of the wave vector of the incident THz wave along the x-direction and can be defined as (c is the speed of light in vacuum)

$$\overrightarrow{k}_{x} = \begin{cases} k_{//}(1,0,0) & \Gamma M \\ k_{//}\left(1, \dfrac{1}{\sqrt{3}}, 0\right) & \Gamma K \end{cases}, \quad (2)$$

here $k_{//}$ represents incident amplitude of parallel momentum. G_x and G_y are the PC momentum for hexagonal lattice and can be expressed as

$$\overrightarrow{G}_{x} = \frac{2\pi}{p}\left(\frac{2}{\sqrt{3}}, 0, 0\right), \quad (3)$$

$$\overrightarrow{G}_{y} = \frac{2\pi}{p}\left(\frac{1}{\sqrt{3}}, 1, 0\right). \quad (4)$$

Then Eq.(1) can be rewritten as:

$$|\overrightarrow{k}_{sur}| = \begin{cases} \left[\left(k_{//} + m\frac{2\pi}{p}\cdot\frac{2}{\sqrt{3}} + n\frac{2\pi}{p}\cdot\frac{1}{\sqrt{3}}\right)^2 + \left(n\frac{2\pi}{p}\right)^2\right]^{1/2} & \Gamma M \\ \left[\left(k_{//} + m\frac{2\pi}{p}\cdot\frac{2}{\sqrt{3}} + n\frac{2\pi}{p}\cdot\frac{1}{\sqrt{3}}\right)^2 + \left(\frac{k_{//}}{\sqrt{3}} + n\frac{2\pi}{p}\right)^2\right]^{1/2} & \Gamma K \end{cases}. \quad (5)$$

In an out-of-plane scheme, the silicon PC slab is capable of supporting guided resonances, which can either leak out of the plane of the slab or trap inside the slab. They have finite lifetime inside the slab due to coupling to external propagating modes, and can be excited by using external waves [3]. For the metal PC slab, however, these guided resonances have been described as SP resonances, which can be localized at the interface between metal and air, and can also couple to free space modes. In the limit that the air hole diameter shrinks to zero, i.e., in the empty lattice approximation, the wave vector on the surface can be expressed as

$$\left|\overrightarrow{k}_{sur}\right| = \left|\overrightarrow{k}_{sp}\right| = \frac{2\pi f_{sp}}{c}\sqrt{\frac{\varepsilon_1\varepsilon_2}{\varepsilon_1+\varepsilon_2}}, \quad (6)$$

where $\overrightarrow{k}_{sp}$ is the surface plasmon resonance vector and f_{sp} is the resonant frequency of SP; ε_1 is the permittivity of the surrounding material and $\varepsilon_2 = \varepsilon_{r2} + i\varepsilon_{i2}$ is the permittivity of the metal-like grating materials (ε_{r2} and ε_{i2} are the real and imaginary parts, respectively). The permittivity of Al at around 1 THz is about $\varepsilon_2 = -44900 + i511000$ [13], which is much larger than that in visible range [18]. Therefore we can approximate $(\varepsilon_1\varepsilon_2/(\varepsilon_1+\varepsilon_2))^{1/2} \approx 1$ in Eq. (6).

Fig. 4(a) and (b) shows the band dispersions for the metal PC in the ΓM and ΓK directions as a function of the parallel momentum wave number according to Eqs. (5) and (6). For convenience, both dispersion diagrams are folded into the first Brillouin zone. In Fig. 4(a), one strong transmission peak line (red line) and three

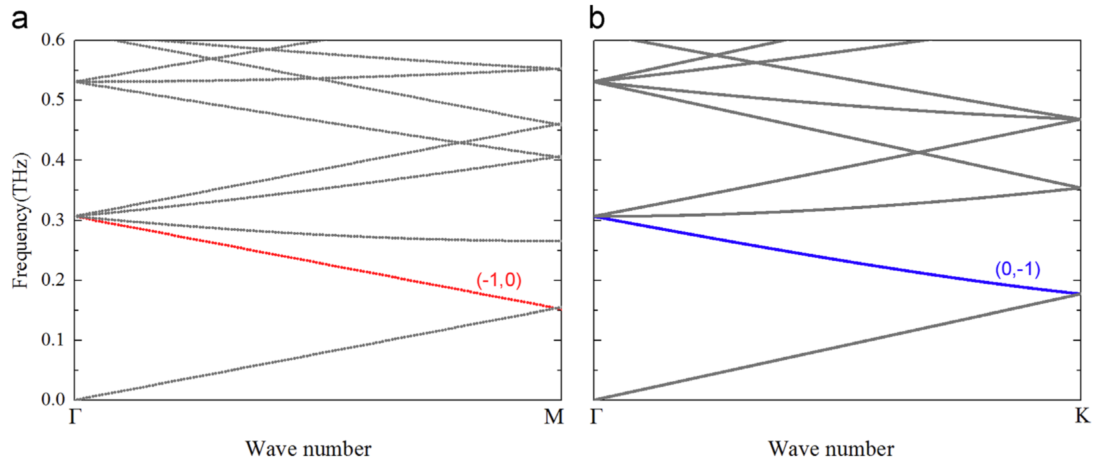

Fig. 4. Photonic band diagrams for metal PC with (a) the ΓM direction and (b) the ΓK direction. Red line: dominant mode $(-1, 0)$ in the ΓM direction; Blue line: dominant mode $(0, -1)$ in the ΓK direction. (For interpretation of the references to color in this figure legend, the reader is referred to the web version of this article.)

weak peak lines are observed. The red line corresponds to the dominant SP mode $(-1, 0)$. We find that $(-1, 0)$ mode has the steep negative gradient which is almost the same value with that of light in vacuum. In Fig. 4(b), however, there are one strong peak line (blue line) and two weak peak lines. The blue line corresponds to the dominant SP mode $(0, -1)$. The gradient of the $(0, -1)$ mode is similar to that of $(-1, 0)$ mode in Fig. 4(a).

From Eqs. (5) and (6), we can see that the resonant frequency f_{sp} of SP is influenced not only by the geometrical configuration of the hole arrays but also by the incident angle θ. It is obvious that $k_{//}$ can be expressed as

$$k_{//} = \left|\vec{k}_{sp}\right| \sin\theta = \frac{2\pi f_{sp}\sin\theta}{c}\sqrt{\frac{\varepsilon_1\varepsilon_2}{\varepsilon_1+\varepsilon_2}} \approx \frac{2\pi f_{sp}\sin\theta}{c}. \tag{7}$$

Substituting Eqs. (6) and (7) into Eq. (5), we get

$$\left(\frac{2\pi}{c}f_{sp}\sin\theta + m\cdot\frac{2\pi}{c}\cdot\frac{2c}{p\sqrt{3}} + \frac{n}{2}\cdot\frac{2\pi}{c}\cdot\frac{2c}{p\sqrt{3}}\right)^2 + \left(n\cdot\frac{\sqrt{3}}{2}\cdot\frac{2\pi}{c}\cdot\frac{2c}{p\sqrt{3}}\right)^2 = \left(\frac{2\pi f_{sp}}{c}\right)^2, \quad \Gamma\text{M} \tag{8}$$

and

$$\left(\frac{2\pi}{c}f_{sp}\sin\theta + m\frac{2\pi}{c}\frac{2c}{p\sqrt{3}} + \frac{n}{2}\frac{2\pi}{c}\frac{2c}{p\sqrt{3}}\right)^2 + \left(\frac{2\pi}{c}\frac{f_{sp}}{\sqrt{3}}\sin\theta + n\frac{\sqrt{3}}{2}\frac{2\pi}{c}\frac{2c}{p\sqrt{3}}\right)^2 = \left(\frac{2\pi f_{sp}}{c}\right)^2. \quad \Gamma\text{K} \tag{9}$$

If we define the lowest SP resonant frequency at normal incidence f_0 and normalized resonant frequency u as

$$f_0 = \frac{2c}{p\sqrt{3}}, \text{ and } u = \frac{f_{sp}}{f_0}, \tag{10}$$

then Eqs. (8) and (9) can be rewritten as

$$\left(u\sin\theta + m + \frac{n}{2}\right)^2 + \left(n\frac{\sqrt{3}}{2}\right)^2 = u^2, \quad \Gamma M \tag{11}$$

and

$$\left(u\sin\theta + m + \frac{n}{2}\right)^2 + \left(\frac{u\sin\theta}{\sqrt{3}} + n\frac{\sqrt{3}}{2}\right)^2 = u^2 \quad \Gamma K \tag{12}$$

After some calculations, we obtain

$$u^2\cos^2\theta - u\sin\theta(2m+n) - (m^2+mn+n^2) = 0, \quad \Gamma\text{M} \tag{13}$$

and

$$u^2\left(1 - \frac{4}{3}\sin^2\theta\right) - 2(m+n)\cdot u\cdot\sin\theta - (m^2+mn+n^2) = 0. \quad \Gamma\text{K} \tag{14}$$

The solutions for these quadratic equations are

$$u = \frac{2(m^2+mn+n^2)}{\sqrt{(2m+n)^2+3n^2\cos^2\theta} - (2m+n)\sin\theta}, \quad \Gamma\text{M} \tag{15}$$

and

$$u = \frac{m^2+mn+n^2}{\sqrt{m^2+mn+n^2-(1/3)(m-n)^2\sin^2\theta} - (m+n)\sin\theta}. \quad \Gamma\text{K} \tag{16}$$

Using Eqs. (10), (15) and (16), we can obtain the resonant frequencies for SP

$$f_{sp} = \frac{2(m^2+mn+n^2)}{\sqrt{(2m+n)^2+3n^2\cos^2\theta} - (2m+n)\sin\theta}\cdot f_0, \quad \Gamma\text{M} \tag{17}$$

and

$$f_{sp} = \frac{m^2+mn+n^2}{\sqrt{m^2+mn+n^2-(1/3)(m-n)^2\sin^2\theta} - (m+n)\sin\theta}\cdot f_0 \quad \Gamma\text{K} \tag{18}$$

According to Eqs. (17) and (18), the resonant frequencies f_{sp} for the strong SP modes $(-1,0)$ (ΓM) and $(0,-1)$ (ΓK) are simplified in the form:

$$f_{sp}(\theta) = \begin{cases} \dfrac{f_0}{\sin\theta+1} & \Gamma M \\ \dfrac{f_0}{\sin\theta + \sqrt{1-(1/3)\sin^2\theta}}. & \Gamma K \end{cases} \tag{19}$$

The experimental and theoretical results (Eqs. (17) and (18)) of the dependence of the resonant frequency f_{sp} on the incident angle are shown in Fig. 5. It is evident that the resonances shift to lower frequencies as the incident angle increases. The dispersions are results of the folding of the in-plane Brillouin zone, which can lead to negative values of $df/d\theta$ (or $d\omega/dk_{//}$). Thus, the dispersion curves are now able to interact with the electromagnetic plane waves that come from outside. The theoretical results according to Eqs.(17) and (18) show good agreement with the experimental results.

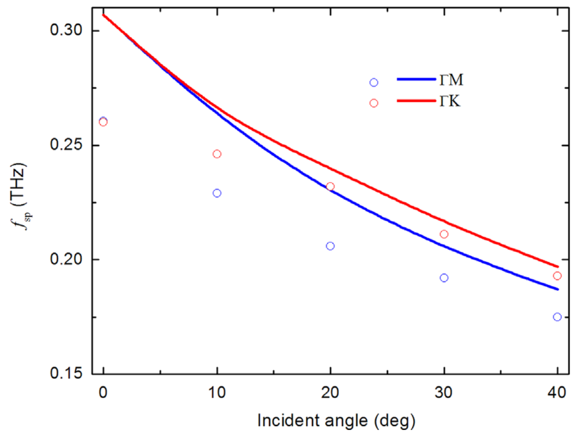

Fig. 5. Experimental (dots) and theoretical (lines) resonant frequency as a function of incident angle for dominant modes in the ΓM and ΓK directions.

The discrepancy of the measured resonant frequency with the theoretical value can be described by the following reason. Eq. (6) is an approximation for metal surface using SP dispersion appropriate for a flat surface. The sample in this system is made of metal with periodic holes on it, which might modify the SP dispersion curve in Eq.(6) to some extent. According to Pendry's theory [19], as the metal area decreases (the surface of metal is periodically structured), the attenuation length becomes shorter and the electric field of SP wave can be localized more strongly on the metal surface. Thus, the effective permittivity of the metal PC surface increases, leading to the fact that the measured resonant frequency is lower than that expected from Eqs. (17) and (18). Another reason of the discrepancy might arise from imperfections in the fabrication. In addition, Fig. 5 also shows that the value between the theoretical and experimental results decreases as the incident angle increases. This is due to the increase of the in-plane wave-vector component of the incident wave. For example, according to Eq. (1), the difference Δ between the theoretical and experimental results for SP mode $(-1, 0)$ (ΓM) can be roughly described as

$$\Delta \propto \frac{\sqrt{\varepsilon_{eff}}-1}{1+\sin\theta} f_0, \tag{20}$$

where ε_{eff} represents the effective permittivity of the metal PC surface and $\varepsilon_{\text{eff}} > 1$. It is clear that the value between the theoretical and experimental results decreases with increasing the incident angle according to Eq. (20).

3. Conclusion

We demonstrate the THz transmission spectra through metal PC by rotating the incident angle around two lattice directions in order to understand photonic band behind these spectra. We found that (1) the strongest resonant frequency shows redshift when the incident angle increases; (2) the transmission spectra rotating along the ΓK directions are different with those rotating along the ΓM directions, which is determined by the incident wave vector at lattice directions. The theoretical results show good agreement with the experimental results. Further research on estimation of relation between enhanced transmission and incident angle will be expected to find applications in THz near-field microscopy, high resolution THz imaging, and tunable THz filters.

Acknowledgment

This work was partly supported by the National Program on Key Basic Research Project of China (973 Program, 2014CB339806), National Natural Science Foundation of China (11174207, 61138001, 61205094, 61307126), Major National Development Project of Scientific Instrument and Equipment (2011YQ150021, 2012YQ14000504), the Key Scientific and Technological Project of Shanghai Municipality (12142200100), Shanghai Rising-Star Program (14QA1403100), Program of Shanghai Subject Chief Scientist (14XD1403000) and Basic Research Key Project (12JC1407100).

Reference

[1] J.M. Lourtioz, H. Benisty, V. Berger, J.M. Gerard, D. Maystre, A. Tchelnokov, Photonic Crystals: Towards Nanoscale Photonic Devices, Springer-Verlag, Berlin Heidelberg, 2005.
[2] A.K. Azad, Y. Zhao, W.L. Zhang, Appl. Phys. Lett. 86 (2005) 141102.
[3] Z.P. Jian, D.M. Mittleman, J Appl. Phys. 100 (2006) 123113.
[4] T. Prasad, V.L. Colvin, D.M. Mittleman, Opt. Express 15 (2007) 16954.
[5] T. Okada, S. Tsuji, K. Tanaka, K. Hirao, K. Tanaka, Appl. Phys. Lett. 97 (2010) 261111.
[6] F. Miyamaru, M. Hangyo, Appl. Phys. Lett. 84 (2004) 2742.
[7] A.P. Hibbins, B.R. Evans, J.R. Sambles, Science 308 (2005) 670.
[8] B. Hou, W.J. Wen, Opt. Express 16 (2008) 17098.
[9] W.L. Zhang, Eur. Phys. J. Appl. Phys. 43 (2008) 1.
[10] F.J. Garcia-Vidal, L. Martin-Moreno, T.W. Ebbesen, L. Kuipers, Rev. Mod. Phys. 82 (2010) 729.
[11] K.J. Wang, L. Ding, J.S. Liu, J. Zhang, X.M. Yang, J.Y. Chin, T.J. Cui, Opt. Express 19 (2011) 11375.
[12] F. Miyamaru, M. Kamijyo, N. Hanaoka, M.W. Takeda, Appl. Phys. Lett. 100 (2012) 081112.
[13] E.K. Stone, E. Hendry, Phys. Rev. B 84 (2011) 035418.
[14] M.K. Liu, Y.J. Song, Y. Shen, Y.B. Zhang, X.H. Wang, C.J. Jin, Plasmonics 7 (2012) 397.
[15] J.M. Xu, L. Chen, L. Xie, S.Q. Du, M.H. Yuan, Y. Peng, Y.M. Zhu, Plasmonics 8 (2013) 1293.
[16] L. Chen, C.M. Gao, J.M. Xu, X.F. Zang, B. Cai, Y.M. Zhu, Opt. Lett. 38 (2013) 1379.
[17] L. Chen, J.M. Xu, C.M. Gao, X.F. Zang, B. Cai, Y.M. Zhu, Appl. Phys. Lett. 103 (2013) 251105.
[18] L. Chen, Z.Q. Cao, F. Ou, H.G. Li, Q.S. Shen, H.C. Qiao, Opt. Lett. 32 (2007) 1432.
[19] J.B. Pendry, L. Martín-Moreno, F.J. Garcia-Vidal, Science 305 (2004) 847.